

SCIENTIFIC REPORTS

OPEN

Pressure-sensitive liquid phase epitaxy of highly-doped n-type SiGe crystals for thermoelectric applications

Hung-Wei Li¹ & Chih-Wei Chang^{1,2} 

Based on recent works, the most desirable high-temperature thermoelectric material would be highly-doped $\text{Si}_{1-x}\text{Ge}_x$ crystals or films with sufficiently high Ge concentrations so that simultaneous enhancing the power factor and wave-engineering of phonons could be possible on the ballistic thermal conductor. However, available thin film deposition methods such as metal organic chemical vapor deposition, electron-beam evaporation, or sputtering are unable to produce highly-doped SiGe single crystals or thick films of high quality. To fabricate the desired material, we here employ liquid phase epitaxy to make highly-doped (up to 2% GaP doping) SiGe crystals with minimized concentration variations on Si (111) and (100) substrates. We find that growing $\text{Si}_{1-x}\text{Ge}_x$ ($x = 0.05\text{--}0.25$) crystals from Ga solvents at relatively high vacuum pressure (0.1 torr) displays significant deviations from previous calculated phase diagram. Moreover, doping GaP into SiGe is found to affect the solubility of the system but not the resulting Ge concentration. We thus plot a new pressure-dependent phase diagram. We further demonstrate that the new pressure-induced liquid phase epitaxy technique can yield $\text{Si}_{1-x}\text{Ge}_x$ crystals of much higher Ge concentrations ($x > 0.8$) than those grown by the conventional method.

Recent experimental discoveries of room temperature ballistic thermal conduction have opened possibilities for engineering wave properties of phonons^{1,2}. Particularly, the ballistic thermal conduction is found to persist over $8\ \mu\text{m}$ at 300 K in homogeneously-alloyed SiGe nanowires¹. The unprecedented microscale ballistic thermal transport would reduce many technical barriers for unraveling many interesting phenomena. The phonons carrying out heat conduction in SiGe are estimated to occupy only 0.04% of the excited phonon spectrum, and most other short-wavelength phonons are localized due to alloy scatterings¹. Hence, although the thermal conductivity of the SiGe nanowires is low ($< 10\ \text{W/m}\cdot\text{K}$), the phonon mean free path is much longer than that of Si nanowires.

On the other hand, SiGe are known to be thermoelectric materials with superior figure of merit ($ZT = \sigma S^2 T / \kappa$, here σ is electrical conductivity, S is the Seebeck coefficient, κ is thermal conductivity, and T is temperature) at high temperatures ($ZT \sim 1$ at $T = 1200\ \text{K}$). The κ of $\text{Si}_{1-x}\text{Ge}_x$ is known to drop very quickly as x increases and the ZT is predicted to reach maximum at $x = 0.5$ ^{3,4}. The microscale ballistic thermal conduction, combined with the thermoelectric properties, would make SiGe useful for realizing next-generation thermoelectric devices inspired by phononic crystals⁵.

Because the dominant low-frequency phonons carrying out the heat conduction are estimated to have wavelengths longer than 10 nm, which is much shorter than the diameters ($\sim 200\ \text{nm}$) of SiGe nanowires, the observed ballistic thermal conduction is suggested to be a bulk property of SiGe¹. Indeed, even though each material has their own ZT characteristics at different temperatures and different synthetic strategies have been applied to enhance ZT ^{6,7}, so far SiGe is a unique material demonstrated to exhibit ballistic thermal conduction for a wide range of alloy concentration. As mentioned above, strong length dependent thermal conductivities have been found in $\text{Si}_{0.9}\text{Ge}_{0.1}$ and $\text{Si}_{0.4}\text{Ge}_{0.6}$ nanowires¹. Thickness dependent thermal conductivity has also been found in $\text{Si}_{0.9}\text{Ge}_{0.1}\text{--}\text{Si}_{0.7}\text{Ge}_{0.3}$ superlattice films^{8,9}. Rowe *et al.* discovered that when the N-type, heavily-doped ($\sim 10^{20}/\text{cm}^3$) $\text{Si}_{0.63}\text{Ge}_{0.26}$ grain size is less than $5\ \mu\text{m}$, 28% reduction of thermal conductivity is observed¹⁰, indicating ballistic thermal conduction remains robust even when electron-phonon interactions could enhance scatterings of low-frequency phonons¹¹. Furthermore, calculations based on density functional theory suggest that ballistic thermal conduction should be longer than $1\ \mu\text{m}$ ¹². Frequency

¹Center for Condensed Matter Sciences, National Taiwan University, Taipei, 10617, Taiwan. ²Center of Atomic Initiative for New Materials (AI-MAT), National Taiwan University, Taipei, 10617, Taiwan. Correspondence and requests for materials should be addressed to C.-W.C. (email: cwchang137@ntu.edu.tw)

dependent time-domain thermal reflectance measurements on bulk $\text{Si}_{0.4}\text{Ge}_{0.6}$ also suggest pronounced contributions from ballistic phonons¹³. These property indicates that large area applications based on the novel ballistic thermal conduction could be realized in SiGe crystals or thick films of microscale thickness. Yet, to experimentally investigate their ballistic thermal conduction, SiGe crystals or films of micrometer thick will be needed. To further realize their thermoelectric applications, highly-doped SiGe films are also required. Unfortunately, commercially available SiGe wafers usually contain Ge concentration less than 10% and cannot meet the unusual doping requirement. In addition, many available thin film techniques, such as metal organic chemical vapor deposition, electron-beam evaporation, or sputtering often yield polycrystalline films. Besides, many post-doping processes are unable to produce highly-doped SiGe films required for optimizing the thermoelectric performance.

Enhancing thermoelectric performance of SiGe by GaP doping was found to give 20~30% improvement of ZT compared to standard P-doping. Vining and Fleurial concluded that the enhancement can be attributed to an increase of carrier concentrations from $2.1 \times 10^{20} \text{ cm}^{-3}$ (0.4% P doped) to $3.3 \times 10^{20} \text{ cm}^{-3}$ (0.4~2% GaP doped) that leads to an improved power factor¹⁴. Grain size effects, which were considered to reduce κ , were suggested to be minimal¹⁴. Yet, recent works employing 2.5% GaP doping on SiGe nanoparticles of 13 nm diameters was found to reach $ZT = 0.95$ at 1200 K and a ten-fold reduction of κ was observed¹⁵. Although the subtleties of increased carrier concentrations and reduced thermal conductivity have not been fully understood, these works indicate the possibilities for further engineering σ and κ in SiGe.

To exploit the ballistic thermal conduction properties in GaP-doped SiGe, high quality crystals will be needed. However, the quaternary compound cannot be easily made by the common thin-film deposition methods. Liquid phase epitaxy (LPE) technique is ideally suited to make the desired highly-doped, single-crystalline SiGe films and crystals. In recent years, LPE has been investigated for applications from solar cell, thermoelectric devices, and to customized epitaxial substrate structures. In particular, the low capital equipment and operating costs; the absence of toxic precursors or byproducts; and producing Si layers with defect densities an order of magnitude lower than that of the Si substrates are the major advantages. Recently, LPE is found to be especially suited for conducting epitaxial lateral overgrowth on patterned or masked substrates for novel device structures^{16,17}.

SiGe crystals or films grown by LPE methods were reported starting in late 1980s¹⁷⁻²⁸. Various solvents including, In¹⁸, Bi²⁰, AuBi²⁹, Sn²⁴, and Ga²⁴ have been used. Good agreements were found between the calculated phase diagram and the ternary systems using Bi as solvents²⁰. However, comparing to the LPE used for making undoped or normally doped SiGe films, literatures on highly-doped SiGe films are scarce. Borshchevsky and Fleurial mentioned unsuccessful attempts to grow SiGe out of Ga-P melts²⁴. They attributed it to complex interactions in the quaternary system. Helped by further adding In into the Ga solvent, they reported successful doping GaP into $\text{Si}_{0.8}\text{Ge}_{0.2}$ crystals by LPE and found that the Ga additions can significantly enhance the P solubility and carrier concentration. In addition, the crystals grown by LPE have lower resistivity than those made by hot-pressed methods. In light of the recent interests in exploring ballistic thermal conduction and its potential applications in thermoelectrics, we find that many of the previous LPE growth conditions and material characterizations of GaP-doped SiGe crystals or films should be clarified. In this paper, we particularly investigate effects that were overlooked by previous works.

The binary solid solution of Si and Ge in various solvents are shown in Fig. 1(a). We see that the solubility of Ge the metal solvents are much more than that of Si. The ternary phase diagram of SiGe in various solvents is obtained from thermodynamic equilibrium model of Malmejac *et al.*³⁰, following Thurmond and Kowalchick's work on binary Si-metal or Ge-metal systems³¹. From the model the Ge concentration (x) in the solid phase of $\text{Si}_{1-x}\text{Ge}_x$ can be expressed as a function of the mole fraction in the liquid phase (x_{liquid}) at saturation temperature (T_{sat}):

$$x \approx \exp \left\{ \frac{1}{RT_{\text{sat}}} \left[\Delta H_{F,Ge} \left(1 - \frac{T_{\text{sat}}}{T_{F,Ge}} \right) + \lambda_{Ge,solvent} \right] \right\} x_{\text{liquid}} \quad (1)$$

Here $\Delta H_{F,Ge} = 8830 \text{ cal/mole}$ is the latent heat of Ge for fusion, $T_{F,Ge} = 1210 \text{ K}$ is melting point of Ge, and $\lambda_{Ge,solvent} = -150$ is the interaction parameter in different solvents^{20,31}. As shown in Fig. 1(b), for a fixed T_{sat} , Bi or Pb favors Ge-rich samples, whereas In or Ga leads to Si-rich samples. Because our goal is to make highly-doped SiGe crystals, we will start from growing undoped SiGe using Ga solvent and then further employing similar conditions for GaP doping.

A tipping boat method was usually employed in earlier works. But, as will be shown later, we found that there were always large amounts of residues sticking to the substrate and could not be easily removed. On the other hand, the sliding boat method, which involved graphite crucible designed for efficient heat exchange at the substrate and *in-situ* temperature monitoring, offered better controllable growth conditions. As shown in Fig. 2(a,b), here a home-made heat exchanger was used for cooling the substrate via pressurized gas with regulated flow rates. The temperature of the substrate was simultaneously monitored by three thermocouples located at different positions during the entire process. We had also varied the cooling rates from $-1 \text{ }^\circ\text{C/min}$ to $0 \text{ }^\circ\text{C/min}$ during the growth. Unlike the tipping boat method, only a thin layer of residues was found in the sliding boat method and could be peeled off from the substrate after cooling it to room temperature. The grown crystals/films were characterized by energy dispersive X-ray spectroscopy (EDS), electron probe microanalysis (EPMA) equipped with wavelength dispersive spectroscopy (WDS), and x-ray electron spectroscopy (XPS).

Results and Discussion

We firstly employ EDS to investigate concentration profiles along the thickness of SiGe crystals/films grown by different LPE methods and cooling rates. For crystals grown on Si (111) surface using the tipping boat method, a thick layer of Ge precipitates is found, whose morphology looks very similar to previous reports and could be mistakenly regarded as SiGe films in early works. Apparently, the unwanted Ge layer comes from residues that stick to the substrate mentioned above that cause the Ge precipitation at low temperature after the furnace is cooled. Cross-sectional EDS and mapping indeed displays that the Ge concentration varies abruptly along the

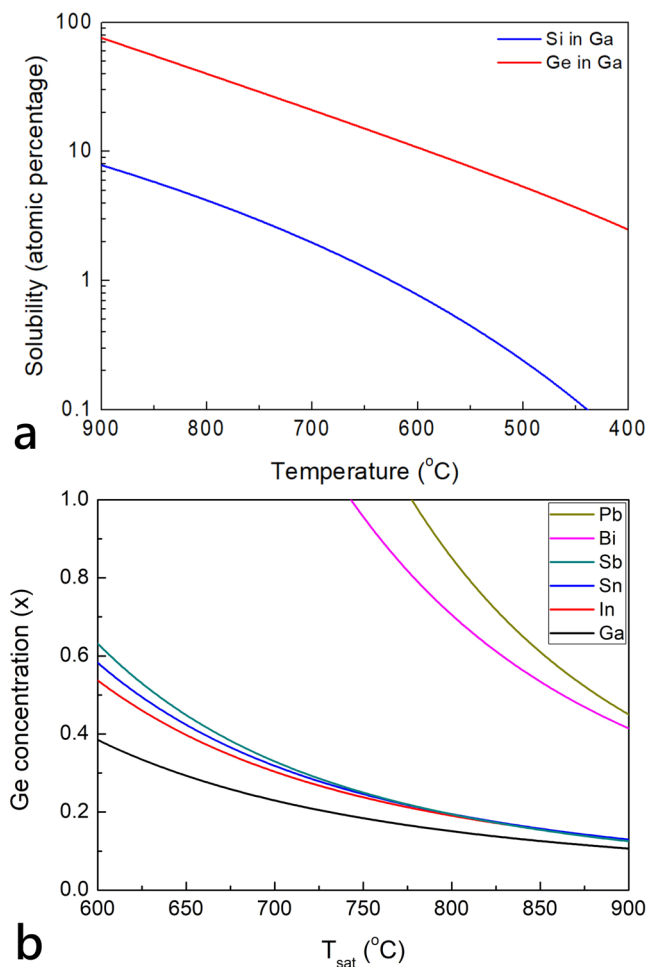


Figure 1. (a) Solubility vs. temperature for Si in Ga (blue curve) and Ge in Ga (red curve). (b) Calculated Ge concentration vs. T_{sat} for different solvents using Eq. (1) with $x_{\text{liquid}} = 0.1$ and the parameters listed in ref.³¹.

thickness. Because the tipping boat method lacks the desired controllability during the growth, we have instead employed sliding boat method later.

Presumably to compensate the material loss in the solvent, a cooling rate with a gradually declined temperature during the growth was often employed by many previous sliding boat methods. Using a cooling rate = $-0.32\text{ }^{\circ}\text{C}/\text{min}$ shown in Fig. 3(a), the cross-sectional EDS shown in Fig. 3(b) displays the concentration profile of a representative grown crystal. We see that the Si concentration gradually decreases with thickness, whereas the Ge concentration steadily increases from 2% at the bottom to 15%, and then abruptly increases to 90% at the top of the crystal. Even though the top layer of Ge can be polished away, we find that there are always gradients of Si and Ge concentrations varying along the thickness of crystals whenever a non-zero cooling rate is employed. Because the Ge loss in the solvent is negligible in our experiment, we believe that the concentration gradient is due to the non-constant cooling rate that induces the increasing Ge concentration with increasing crystal thickness.

To minimize the concentration gradient, we have instead applied a fixed cooling rate = $0\text{ }^{\circ}\text{C}/\text{min}$ during the growth. As shown in Fig. 3(c), here both the temperature of the furnace and the flow rate of the cooling gas are regulated to keep T_{sat} constant. Figure 3(d) displays that the grown $\text{Si}_{1-x}\text{Ge}_x$ crystal on a Si (111) substrate exhibit a much reduced concentration variation ($\Delta x = \pm 0.007$) even when the crystals are more than $20\text{ }\mu\text{m}$ thick. Further EPMA-WDS mapping on another crystal has confirmed the result (see supplementary information).

We have also applied identical growth conditions on Si (100) surfaces. Here the grown SiGe crystals are found to be of pyramidal shapes, as shown in Fig. 3(e). According to Sembian *et al.*²⁵, the pyramidal growth is the result when the Ge concentration increases beyond 13%. Three-dimensional nucleation and growth have been suggested to be associated with the lattice mismatch between the grown layer and the substrate (lattice mismatch for Si/Ge = 4.2%) as well¹⁸. The pyramidal crystals grown on Si (100) sometimes give inhomogeneous Ge concentration distribution within a crystal. The inhomogeneity could originate from the uneven mixtures of Si/Ge in the solvent. Elongating the holding time at T_{high} from 2 to 8 hours indeed minimizes the problem. To reduce the concentration variation along the thickness, we again employ a constant cooling rate during the growth. The concentration variation is minimized, as shown in Fig. 3(e).

After the successful growth of SiGe crystals, we then proceed to do GaP doping. Interestingly, introducing 0.06–0.4% molar fraction (with respect to that of Ga) of P powder is found to significantly perturb the solubility

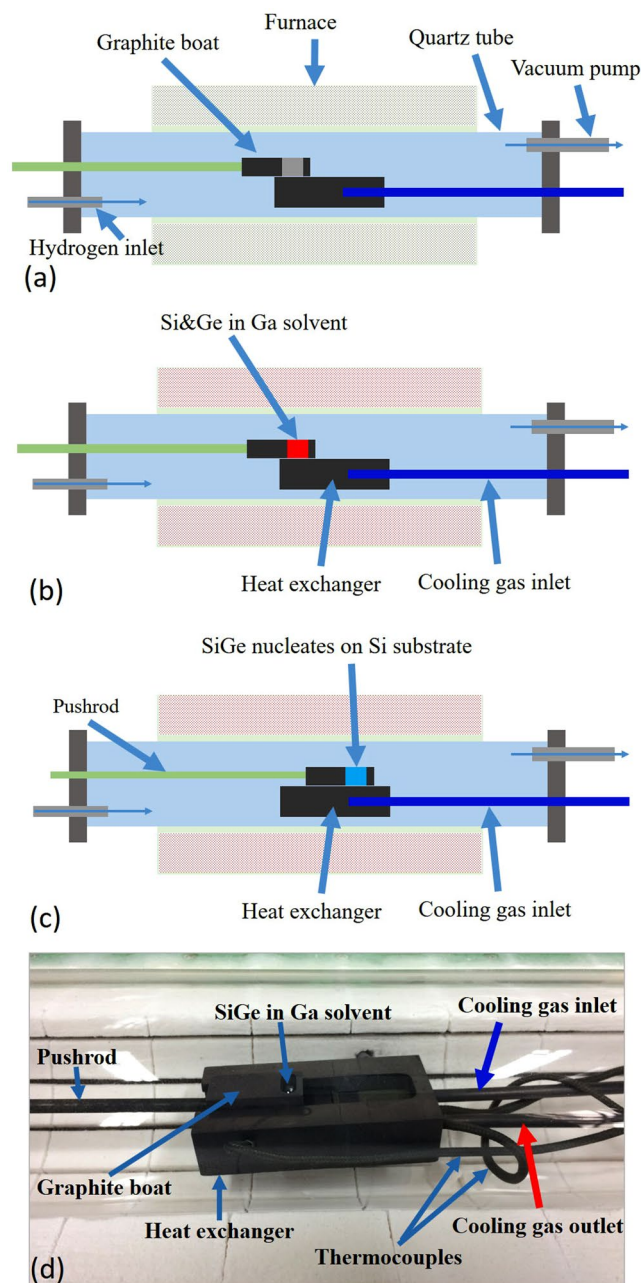


Figure 2. Schematics of LPE procedure (a) A quartz tube was evacuated and then continuously purged with H_2 before raising the temperature of the furnace. (b) After reaching the highest set temperature ($T_{\text{high}} = T_{\text{sat}} + \Delta T$), the temperature was held for more than 2.5 h to homogenize the solution. We then turned on the cooling gas so the heat exchanger and the Si substrate were cooled down to T_{sat} . (c) Using a pushrod to slide the boat and nucleation of the seeds started. The growth time varied from 1.5 to 18 hours. Finally, the growth was terminated by removing the solution away from the substrate (not shown). (d) A photo of the LPE assembly inside a furnace.

of Si and Ge in Ga, and tiny SiGe crystals are found even when identical growth conditions mentioned above are applied. To solve the problem, we have followed Borshevsky and Fleuriat's method and added a small amount (0.18~1.2% molar fraction respect to that of Ga) of In to the system²⁴. However, differing from Borshevsky and Fleuriat's work, we find that higher T_{high} is needed to dissolve the Si and Ge during the growth. The P concentration, as determined by EMPA-WDS, is found to reach more than 0.5%. The $Si_{0.84}Ge_{0.16}$ crystals grown on Si (100) and (111) substrates are also homogeneously alloyed, as shown in Fig. 4(a–d) by EDS and EMPA-WDS mappings.

The samples are further characterized by XPS of core level electrons in Si and Ge. As shown in Fig. 4(e,f), here the XPS spectra are deconvoluted to the doublet of $Si\ 2p_{3/2}$ and $2p_{1/2}$ as well as $Ge\ 3d_{3/2}$ and $3d_{5/2}$. Except that there is a small amount of detectable peak at 102.6 eV indicating the presence of SiO_x on the surface, no other bindings are found in the grown samples.

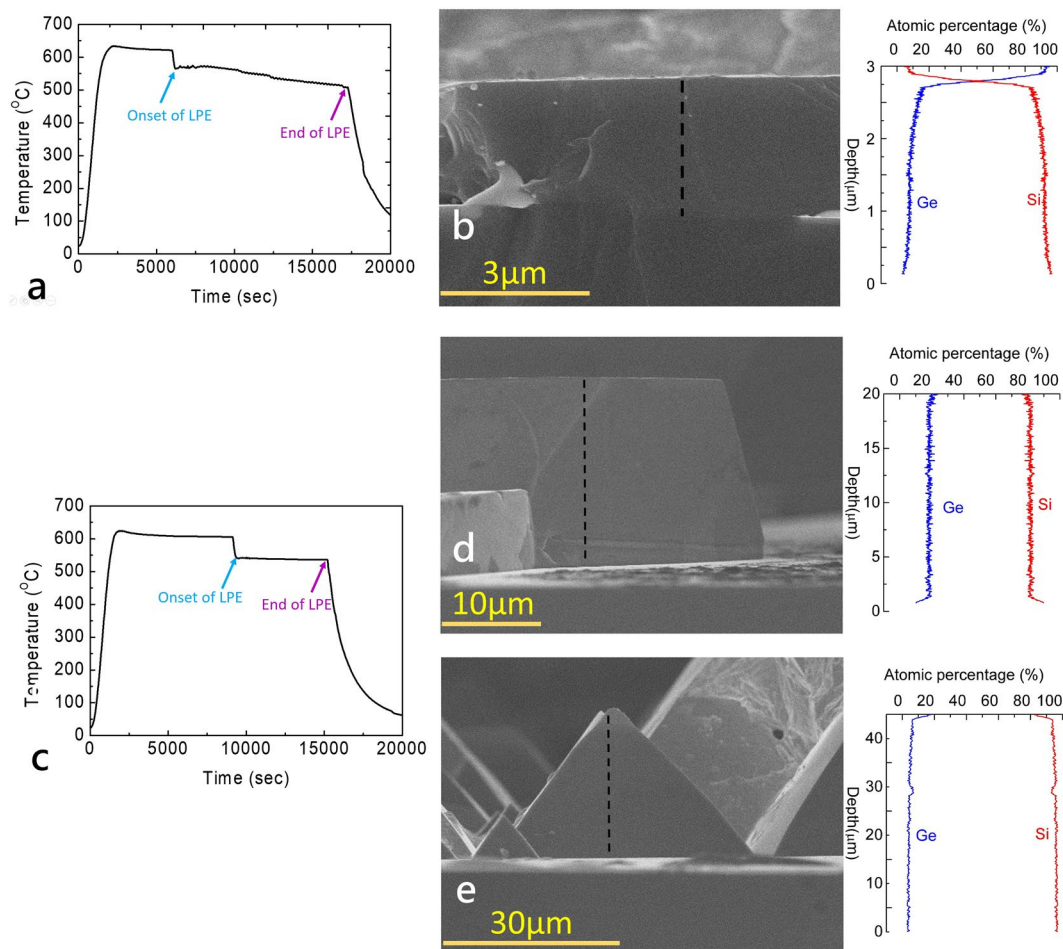


Figure 3. Temperature of a Si substrate vs. time during the LPE process. Here a cooling rate = $-0.32\text{ }^{\circ}\text{C}/\text{min}$ is employed. **(b)** A cross sectional SEM image of the grown SiGe crystal and the corresponding concentration profile determined by EDS. **(c)** Temperature of a Si substrate vs. time during the LPE process. Here a cooling rate = $0\text{ }^{\circ}\text{C}/\text{min}$ is employed. **(d,e)** Cross sectional SEM images and the corresponding concentration profiles of the SiGe crystals grown on **(d)** Si (111) and **(e)** Si (100) surfaces, respectively.

So far we have investigated the relations between Ge concentrations in solid (x), in liquid (x_{liquid}), and T_{sat} for crystals grown at vacuum pressure 0.1 torr. The resulting experimental phase diagram is shown in Fig. 5. First, Fig. 5 shows a pronounced effect that higher x_{liquid} would lead to higher x . Second, lowering T_{sat} tends to yield higher Ge concentration in a crystal. Third, because no apparent deviations are found between Si (100) and (111) substrates, our results demonstrate that the LPE conditions are independent of Si substrates used. Finally, our data display large deviations from the calculated phase diagram. That is, the x measured is usually $\sim 30\%$ lower than the calculated values. In previous works, although agreements between experimental and calculated results were reported when using Bi as a solvent²⁰, $\sim 20\%$ deviation was found when In was used as a solvent¹⁸. Because the calculated curves are obtained from parameters of Si-Ga or Ge-Ga binary systems with an assumption of negligible free energy of mixing, Borshchevsky and Fleuriel have proposed that multicomponent interactions when introducing GaP doping would give substantial deviations from the ternary model²⁴. Interestingly, although our result confirms the large effect of GaP on the solubility of Si and Ge in Ga solvent, Fig. 5 does not display pronounced differences between the undoped and highly-doped SiGe crystals, suggesting that the GaP plays a minor role in the phase diagram.

When varying the H_2 pressure during the growth, we have sometimes found various types of Ge precipitates coexist with SiGe crystals even though they are not anticipated from the phase diagram. As shown in Fig. 6(a-d), diverse morphologies varying from crystals, islands, films, to flakes are found at the surfaces when the pressure is less than 10^{-2} torr. Many of them are found to be Ge precipitation from EDS analyses, but they could be misidentified as the SiGe crystals in previous works. However, employing $\text{HF}:\text{H}_2\text{O}_2:\text{CH}_3\text{COOH} = 1:2:3$ solutions to selectively etch away the unwanted Ge often yields porous materials³², implying poor selectivity. The pressure-dependent morphology changes have not been reported before, and their origin is likely due to some pressure-dependent thermodynamic quantities overlooked by earlier works.

To further elucidate the pressure dependent effects, we have conducted LPE at low vacuum pressures while keeping other conditions unchanged. Figure 7(a) shows the doped and undoped SiGe crystals grown at

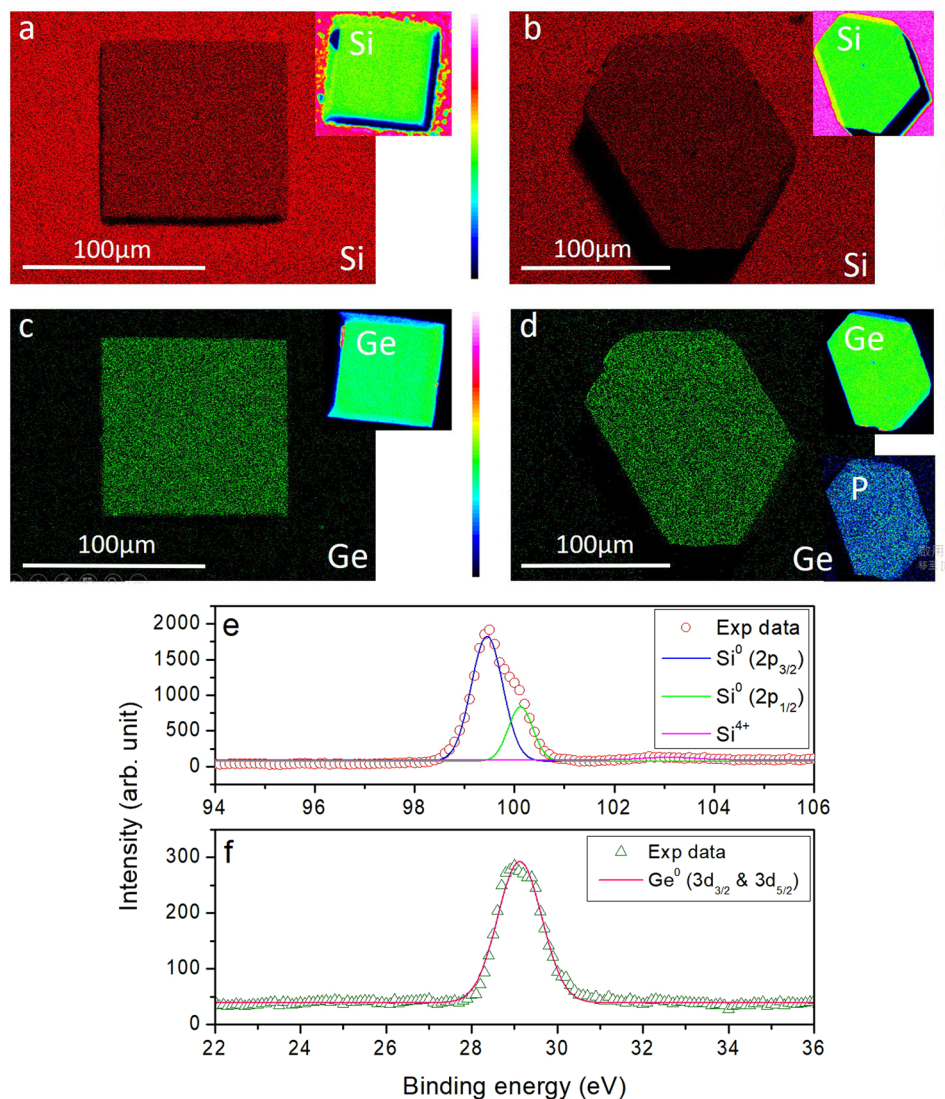


Figure 4. Representative EDS mapping of Si (**a,b**) and Ge (**c,d**) distributions of GaP-doped $\text{Si}_{0.84}\text{Ge}_{0.16}$ crystals grown on a Si (100) substrate (left images) and a Si (111) substrate (right images). The corresponding elemental mappings of EPMA-WDS are shown in the insets, further confirming the Si and the Ge are homogeneously distributed. Here the pyramidal crystal grown on Si (100) has been polished. The P concentration (0.5%) determined by EPMA-WDS shown in the inset of (**d**) also displays homogeneous distribution. (**e,f**) Representative XPS spectra of (**e**) Si $2p$ region and (**f**) Ge $3d$ region of the grown samples.

$T_{\text{sat}} = 580^\circ\text{C}$ under pressure 10^{-5} torr and 10^{-1} torr, respectively. It can be seen that the crystals grown at 10^{-5} torr agree with the calculated curve, suggesting that the thermodynamic parameters used in previous works are applicable to high vacuum only. To directly demonstrate the pressure-induced LPE, Fig. 7(b) shows that we start by setting the initial pressure at 100 torr then quickly pump the pressure to 10^{-5} torr while keeping $T_{\text{sat}} = 580^\circ\text{C}$ throughout the entire process. We have repeated the pressure-induced LPE with different initial Ge/Ga ratios. Interestingly, the resulting $\text{Si}_{1-x}\text{Ge}_x$ crystals always exhibit much higher Ge concentration than those crystals grown by conventional LPE mentioned above and $x = 0.8$ (shown in the inset of Fig. 7(b)) can be found. From the phase diagram shown in Fig. 1(b), $x = 0.8$ can be made only if $T_{\text{sat}} > 775^\circ\text{C}$ and Bi is employed as the solvent. Thus, we demonstrate one key advantage of the novel pressure-induced LPE method. The pressure-induced LPE is a new concept rarely mentioned in previous works. Because pressure is much easier to control than temperature, it has been proposed to improve current LPE methods³³. To our knowledge, our work is the first experimental demonstration of the method. It also points out the important role of regulating pressure during LPE processes.

In summary, we employ LPE to make GaP-doped $\text{Si}_{1-x}\text{Ge}_x$ ($x = 0.05\text{--}0.25$) crystals on Si (111) and (100) substrates. We successfully minimize unwanted concentration variations along the thickness of the grown SiGe crystals via keeping a constant cooling rate. Doping GaP into SiGe is found to affect the solubility of the system but it can be overcome by adding In into the Ga solvent and raising T_{high} of the furnace. The resulting highly-doped SiGe crystals display similar trends like those of undoped crystals in the phase diagram. Yet, we also find that the morphology and the Ge concentration of the grown crystals is sensitively dependent on the vacuum pressure during

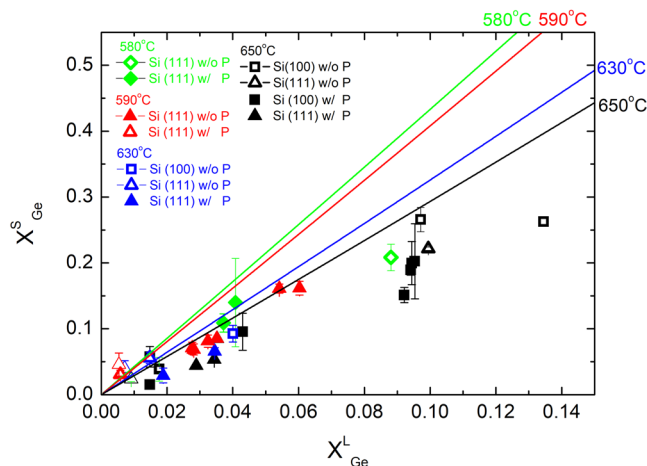


Figure 5. Phase diagram of the relation between Ge concentrations in solid (x) and in liquid (x_{liquid}) for $T_{\text{sat}} = 580^\circ\text{C}$ (green symbols), 590°C (red symbols), 630°C (blue symbols), and 650°C (black symbols) based on our results. The open and solid symbols denote undoped and GaP-doped samples, respectively. The error bars denote the x variations between different crystals. Calculated relationships for $T_{\text{sat}} = 580^\circ\text{C}$ (green line), 590°C (red line), 630°C (blue line), and 650°C (black line) based on Eq. (1) are shown for comparison. It can be seen that the Ge concentrations of our SiGe crystals are always less than the calculated results and deviate from the model by more than 30%.

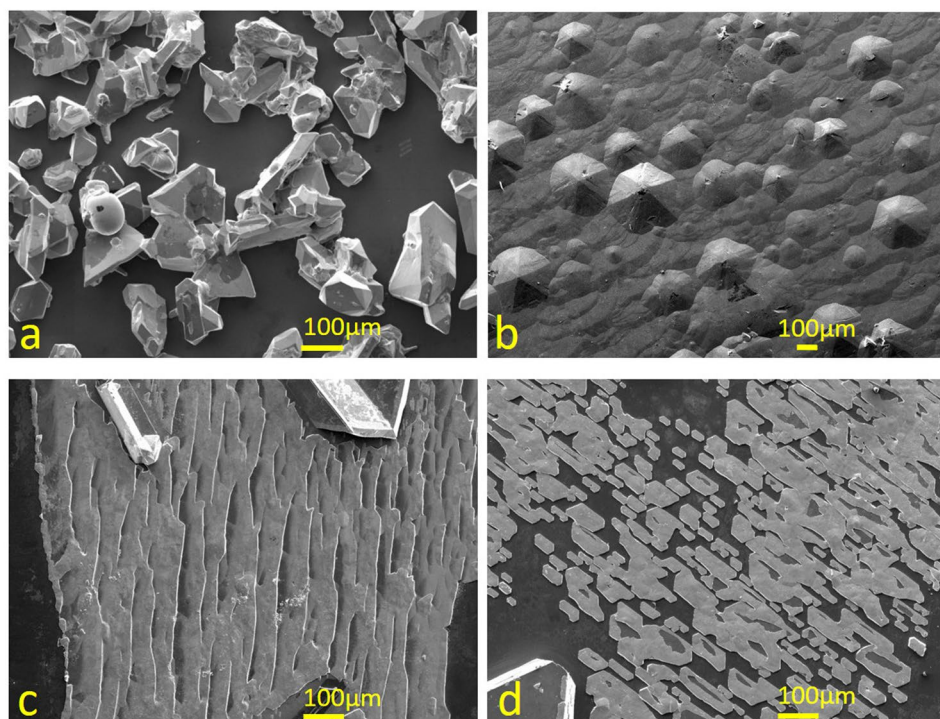


Figure 6. SEM images of different morphologies of high Ge concentration (a) crystals, (b) islands, (c) films, and (d) flakes commonly coexist with other SiGe crystals when LPE is conducted at pressure less than 10^{-2} torr.

the growth. Significant deviations to the calculated phase diagram are found, which are attributed to an overlooked pressure-dependent effect. New pressure-dependent phase diagrams are plotted based on our results at 10^{-1} torr and 10^{-5} torr in Figs 5 and 7(a), respectively. Finally, we directly employ a pressure-induced LPE method to grow $\text{Si}_{1-x}\text{Ge}_x$ crystals and find the crystals exhibit much higher Ge concentrations than those grown by the conventional method.

Methods

Experimentally, Si (111) and (100) substrates were cleaned using acetone, methanol and piranha solution ($\text{H}_2\text{SO}_4:\text{H}_2\text{O}_2 = 3:1$) followed by BOE etchant solution ($\text{HF}/\text{NH}_4\text{F} = 34.6\% / 7.3\%$) etching to remove SiO_2 and rinsing with deionized water. High purity Si (6N) and Ge (6N) powders were mixed with solvent Ga (6N) in a graphite crucible. A quartz tube was evacuated below 10^{-5} torr and then continuously purged with H_2 at a

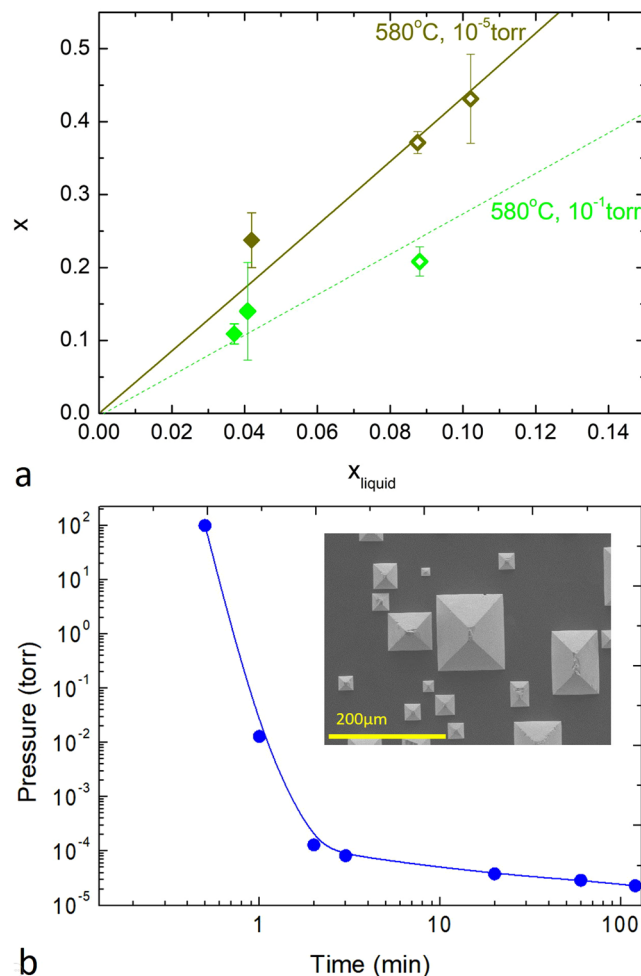


Figure 7. (a) Phase diagram for doped (solid symbols) and undoped (open symbols) SiGe crystals grown at $T_{\text{sat}} = 580^\circ\text{C}$ under pressure 10^{-5} torr (dark yellow symbols) and 10^{-1} torr (green symbols), respectively. The dark yellow curve is the calculated result based on Eq. (1). The dotted green line is a fitted line for crystals grown at $T_{\text{sat}} = 580^\circ\text{C}$ under pressure 10^{-1} torr. (b) Pressure vs. time when conducting pressure-induced LPE at $T_{\text{sat}} = 580^\circ\text{C}$. (Inset) A representative SEM image of the grown Si_{0.2}Ge_{0.8} crystals.

set pressure using a precision leak valve during the entire process. After reaching the highest set temperature ($T_{\text{high}} = T_{\text{sat}} + \Delta T$), the temperature was held for more than 2.5 h to homogenize the solution. We then carried out the LPE using either tipping boat or sliding boat methods. The growth process involved the dissolution of Si and Ge by the Ga melt, nucleation of the seeds at T_{sat} by rapidly cooling the substrate ΔT below T_{high} , and separation of the growth layer from the melt. The growth time varied from 1.5 to 18 hours. Finally, the growth was terminated by removing the solution away from the substrate. After cooling the system to room temperature, excess Ga on the substrate was removed by adding Al foils in hot water. Similar procedures were used for GaP-doping as well, in which high purity P (5N) was mixed with the solvent at the beginning.

References

- Hsiao, T. K. *et al.* Observation of room temperature ballistic thermal conduction persisting over 8.3 micrometers in SiGe nanowires. *Nature Nanotech.* **8**, 534–538 (2013).
- Hsiao, T. K. *et al.* Micron-scale ballistic thermal conduction and suppressed thermal conductivity in heterogeneously-interfaced nanowires. *Phys. Rev. B* **91**, 035406 (2015).
- Chen, J., Zhang, G. & Li, B. W. Tunable thermal conductivity of Si_{1-x}Ge_x nanowires. *Appl. Phys. Lett.* **95**, 073117 (2009).
- Shi, L. H., Yao, D. L., Zhang, G. & Li, B. W. Large thermoelectric figure of merit in Si_{1-x}Ge_x nanowires. *Appl. Phys. Lett.* **96**, 173108 (2010).
- Maire, J. *et al.* Heat conduction tuning by wave nature of phonons. *Sci Adv* **3**, e1700027 (2017).
- Yazdani, S. & Pettes, M. T. Nanoscale self-assembly of thermoelectric materials: a review of chemistry-based approaches. *Nanotechnology* **29** (2018).
- He, J. & Tritt, T. M. Advances in thermoelectric materials research: Looking back and moving forward. *Science* **357**, eaak9997 (2017).
- Huxtable, S. T. *et al.* Thermal conductivity of Si/SiGe and SiGe/SiGe superlattices. *Appl. Phys. Lett.* **80**, 1737–1739 (2002).
- Cheaito, R. *et al.* Experimental Investigation of Size Effects on the Thermal Conductivity of Silicon-Germanium Alloy Thin Films. *Phys. Rev. Lett.* **109**, 195901 (2012).
- Rowe, D. M., Shukla, V. S. & Savvides, N. Phonon-Scattering at Grain-Boundaries in Heavily Doped Fine-Grained Silicon-Germanium Alloys. *Nature* **290**, 765–766 (1981).

11. Liao, B. L. *et al.* Significant Reduction of Lattice Thermal Conductivity by the Electron-Phonon Interaction in Silicon with High Carrier Concentrations: A First-Principles Study. *Phys. Rev. Lett.* **114**, 115901 (2015).
12. Garg, J., Bonini, N., Kozinsky, B. & Marzari, N. Role of Disorder and Anharmonicity in the Thermal Conductivity of Silicon-Germanium Alloys: A First-Principles Study. *Phys. Rev. Lett.* **106**, 045901 (2011).
13. Koh, Y. K. & Cahill, D. G. Frequency dependence of the thermal conductivity of semiconductor alloys. *Phys. Rev. B* **76**, 075207 (2007).
14. Vining, C. & Fleurial, J. F. In *the Tenth Int. Conf. on Thermoelectrics*. (ed. Rowe, D. M.) 1 (Barbrow Press, 1991).
15. Zhu, G. H. *et al.* Increased Phonon Scattering by Nanograins and Point Defects in Nanostructured Silicon with a Low Concentration of Germanium. *Phys. Rev. Lett.* **102**, 196803 (2009).
16. Shimura, T. *et al.* Enhancement of photoluminescence from n-type tensile-strained GeSn wires on an insulator fabricated by lateral liquid-phase epitaxy. *Appl. Phys. Lett.* **107**, 221109 (2015).
17. O'Reilly, A. J. & Quitoriano, N. Asymmetric, compressive, SiGe epilayers on Si grown by lateral liquid-phase epitaxy utilizing a distinction between dislocation nucleation and glide critical thicknesses. *J. Cryst. Growth* **482**, 15–22 (2018).
18. Alonso, M. I. & Bauser, E. Growth of Si_{1-x}Ge_x on Silicon by Liquid-Phase Epitaxy. *J. Appl. Phys.* **62**, 4445–4449 (1987).
19. Hansson, P. O., Werner, J. H., Tapfer, L., Tilly, L. P. & Bauser, E. Liquid-Phase Epitaxy and Characterization of Si_{1-x}Ge_x Layers on Si Substrates. *J. Appl. Phys.* **68**, 2158–2163 (1990).
20. Trah, H. P. Liquid-Phase Epitaxy in the Ternary-System Si-Ge-Bi. *J. Cryst. Growth* **102**, 175–182 (1990).
21. Healy, S. A., Young, T. L. & Green, M. A. Low-Temperature Growth of Silicon on Si_{1-x}Gax by Liquid-Phase Epitaxy. *J. Cryst. Growth* **112**, 287–290 (1991).
22. Chan, B. O., Healy, S. A. & Green, M. A. Strained Si_{1-x}Ge_x Layers Grown by Low-Temperature Liquid-Phase Epitaxy. *Mater. Lett.* **14**, 263–267 (1992).
23. Chen, J. X., Ernst, F., Hansson, P. O. & Bauser, E. Liquid-Phase Epitaxy of GeSi on (111) Si Substrates - Lattice Defect Structure and Electronic-Properties. *J. Cryst. Growth* **118**, 452–460 (1992).
24. Borshchevsky, A. & Fleurial, J. P. Growth of Heavily-Doped SiGe from Metallic Solutions. *J. Cryst. Growth* **128**, 331–337 (1993).
25. Sembian, A. M. *et al.* Defect distribution and morphology development of SiGe layers grown on Si(100) substrates by LPE. *Thin Solid Films* **336**, 116–119 (1998).
26. Fuller, T., Konuma, M., Zipprich, J. & Banhart, F. The critical thickness of silicon-germanium layers grown by liquid phase epitaxy. *Appl. Phys. A* **69**, 597–603 (1999).
27. Sazaki, G. *et al.* In-situ monitoring system of the position and temperature at the crystal-solution interface. *J. Cryst. Growth* **236**, 125–131 (2002).
28. Schade, M. *et al.* Investigation of the chemical composition profile of SiGe/Si(001) islands by analytical transmission electron microscopy. *Appl. Phys. Lett.* **90** (2007).
29. Lee, S. H., Healy, S. A., Young, T. L. & Green, M. A. Very-Low-Temperature Liquid-Phase Epitaxial-Growth of Silicon. *Mater. Lett.* **9**, 53–56 (1990).
30. Malméjac, Y., Bonnier, E. & Desre, P. Contribution to Study of Ternary Ge-Si-Sb Phase-Diagram. *Mem Etud Sci Rev Met* **69**, 565–& (1972).
31. Thurmond, C. D. & Kowalchik, M. Germanium and Silicon Liquidus Curves. *Bcl] Syst. Tech. J.* **39**, 169–204 (1960).
32. Hollander, B., Buca, D., Mantl, S. & Hartmann, J. M. Wet Chemical Etching of Si, Si_{1-x}Ge_x, and Ge in HF:H₂O₂:CH₃COOH. *J. Electrochem. Soc.* **157**, H643–H646 (2010).
33. Mao, X.-J., Chan, Y.-C., Lam, Y.-L., Zhu, J.-Y. & Shi, J. X. New concept technology: pressure variation liquid phase epitaxy. *Proc. SPIE* **4078**, 191–202 (2000).

Acknowledgements

This work is supported by the Ministry of Science and Technology of Taiwan (MOST 104-2628-M-002-010-MY4 and 105-2628-E-006-003-MY3), National Taiwan University (NTU- 107L9008), Center for Sustainability Science of Academia Sinica and Center of Atomic Initiative for New Materials (AI-Mat), National Taiwan University, from the Featured Areas Research Center Program within the framework of the Higher Education Sprout Project by the Ministry of Education in Taiwan. The authors also thank Ms. Joice Ji and Mr. Chung-Yuan Kao of the Instrumentation Center at National Taiwan University for their assistance on EDS and EPMA, respectively.

Author Contributions

H.W.L. designed and conducted the experiment. C.W.C. initiated the project, supervised the whole work, and wrote the manuscript. All authors contributed to discussion and correction for the manuscript.

Additional Information

Supplementary information accompanies this paper at <https://doi.org/10.1038/s41598-019-39786-y>.

Competing Interests: The authors declare no competing interests.

Publisher's note: Springer Nature remains neutral with regard to jurisdictional claims in published maps and institutional affiliations.



Open Access This article is licensed under a Creative Commons Attribution 4.0 International License, which permits use, sharing, adaptation, distribution and reproduction in any medium or format, as long as you give appropriate credit to the original author(s) and the source, provide a link to the Creative Commons license, and indicate if changes were made. The images or other third party material in this article are included in the article's Creative Commons license, unless indicated otherwise in a credit line to the material. If material is not included in the article's Creative Commons license and your intended use is not permitted by statutory regulation or exceeds the permitted use, you will need to obtain permission directly from the copyright holder. To view a copy of this license, visit <http://creativecommons.org/licenses/by/4.0/>.

© The Author(s) 2019